LOW REYNOLDS NUMBER PERFORMANCE OF A MODEL SCALE T-FOIL

(DOI No: 10.3940/rina.ijme.2015.a3.336)

J AlaviMehr, M R Davis, J Lavroff, University of Tasmania, Australia

SUMMARY

Submerged T-foils are an essential forward component of the ride control systems of high speed ferries. A model scale T-Foil for a 2.5m towing tank model of a 112m INCAT Tasmania high-speed wave-piercer catamaran has been tested for both static and dynamic lift performance. The tests were carried out using a closed-circuit water tunnel to investigate the lift and drag characteristics as well as frequency response of the T-Foil. The model T-Foil operates at a Reynolds number of approximately 10^5, has an aspect ratio of 3.6 and a planform which is strongly tapered from the inboard to outboard end. All of these factors, as well as strut and pivot interference, influence the steady lift curve slope ($\frac{dC_L}{d\alpha}$) of the model T-foil which was found to be 61% of the value for an ideal aerofoil with elliptic loading. The T-foil dynamic performance was limited primarily by the stepper motor drive system and connection linkage. At the frequency of maximum motion of the 2.5 m catamaran model (about 1.5Hz) the model T-foil has approximately 5% reduction of amplitude and 15 degrees of phase shift relative to the low frequency response. Only very small limitations arose due to the unsteady lift as predicted by the analysis of Theodorsen. It was concluded that the model scale T-foil performed adequately for application to simulation of a ride control system at model scale.

NOMENCLATURE

a	Dimensionless parameter which determines the location of a point that vertical motion of T-Foil is referenced to
AR	T-Foil Aspect ratio
b	T-Foil semi-chord length (m)
C_D	T-Foil drag coefficient
C_L	T-Foil lift coefficient
$C_{L\alpha}$	T-Foil lift-coefficient derivative ($\frac{dC_L}{d\alpha}$)
D	T-Foil drag force (N)
f	T-Foil Actuation frequency (Hz)
F_y	Load-cell output voltage in the horizontal y-axis direction (V)
F_z	Load-cell output voltage in the vertical z-axis direction (V)
h	T-Foil vertical displacement (m)
$\dot{h}$	T-Foil vertical velocity (m/s)
$\ddot{h}$	T-Foil vertical acceleration (m/s^2)
k	T-Foil Reduced frequency ($\frac{b\omega}{V}$)
L	T-Foil lift force (N)
L/D	T-Foil Lift-to-drag ratio
S	T-Foil planform area (m^2)
V	Water Flow velocity (m/s)
V_{out}	Potentiometer output voltage (V)
V_{in}	Stepper-motor input voltage (V)
α	T-Foil pitch angle of attack (degree)
$\dot{\alpha}$	T-Foil pitch angular velocity (degree/s)
$\ddot{\alpha}$	T-Foil pitch angular acceleration (degree/s^2)
ω	T-Foil Actuation angular frequency ($2\pi f$)
ρ	Water density (kg/m^3)

1. INTRODUCTION

A number of large high-speed and lightweight marine vessels have been developed in the last 25 years in order to satisfy fast sea transportation requirements. Catamaran vessels have proved to be particularly popular among different types of high-speed craft due to their large deck area, relatively large deadweight, high hydrodynamic stability and their ability to provide lightweight Ro-Ro vessels. A unique configuration of high-speed wave-piercing catamarans has been developed by INCAT Tasmania [1] with a prominent centre bow located at the vessel centreline between the wave-piercer demihulls.

High-speed catamarans often experience large heave and pitch motions and high motion accelerations due to their hull shape and operating speed. Increases in vessel speed have generally led to an increase in vessel motions, this leading to poor passenger comfort and potential structural damage while operating in severe sea conditions [2, 3]. A motion control system is therefore required to reduce these large motions and improve the vessel performance.

INCAT Tasmania has applied the use of motion control systems to its high-speed wave piercing catamarans to reduce vessel motions and dynamic structural loads [4, 5]. These motion controls consist of a centre bow mounted T-Foil and active trim tabs located at the stern of the vessel. Figure 1 shows the location of the T-Foil and the trim tabs on the 112 m INCAT Tasmania catamaran vessel [1]. The trim tabs installed on the stern, otherwise known as stern tabs, produce a lift force at the transom of the vessel to keep the vessel on a level trim. Working together, tabs can also control the roll motion of the vessel. The T-Foil installed on the aft section of the centre bow acts to generate a force resisting pitch and heave motion in combination with the stern tabs.

Although some investigations into ship motions as well as motion control systems of INCAT Tasmania vessels have been undertaken through full-scale testing and numerical computations [2-4, 6-9], the mechanisms for the whole motion control system are poorly understood. For optimization of the motion control system further investigation is required to determine the effect of the control system on the ship motions and loads. In

particular, it is not clear what is the best control algorithm for linking detected ship motions to control surface activity.

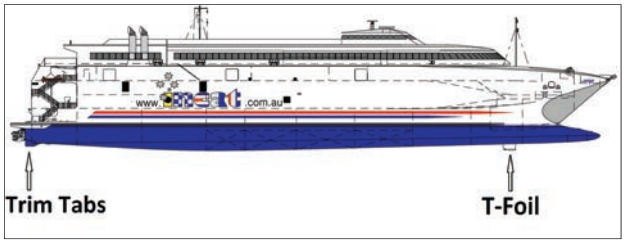

Figure 1: Location of the T-Foil and the trim tabs on the 112m INCAT Tasmania catamaran vessel [1].

Although an active ride control system is installed in the 112m INCAT Tasmania wave-piercer catamaran, the 2.5m hydroelastic segmented model used for model tests [10] does not currently include an active ride control system. Trim tabs are installed in the model but they are statically mounted and no T-foil is currently fitted. Therefore a model scale T-foil has been developed to fit to the model. Figure 2 shows a photo of the electrically activated model T-foil. The overall aim of the model scale ride control system is the evaluation of the effect of ride controls on motions and loads at model scale under more controlled conditions than is possible at full scale. Model scale motions and loads data, in conjunction with numerical computations and full scale sea trials data will ultimately assist in the optimisation of motion control system algorithms, leading to improved ship motions, passenger comfort and reduced structural loads. Full-scale data of foil and tab loads is difficult to measure and so is not available as it has not been measured directly.

In order to optimise the ride control system and design an appropriate algorithm to control ship motion, it is necessary to effectively activate the control surfaces according to vessel response. Some studies of the lifting performance of model scale trim tabs have been undertaken at the University of Tasmania [6, 9]. The present work investigates the lift and drag characteristics as well as frequency response of the model T-Foil by both static and dynamic tests. As the T-Foil is to be used in the ride control system and its angle of attack is to be changed based on the measured unsteady heave and pitch motion and designated algorithms, it is important to conduct dynamic tests on the T-Foil to investigate its performance prior to installation for testing on the 2.5 m hydroelastic catamaran model [11].

Owing to the small scale of the model T-foil it necessarily operates at low Reynolds Number and this creates uncertainty in predicting its lift performance. Predictions of lift performance are also complicated by the relatively low aspect ratio of the planform (AR = 3.6) which tapers strongly towards the foil tips. At a model test speed of approximately 2.7 m/s simulating a full-scale speed of 35 knots the T-Foil Reynolds Number is 105,305 which is sufficiently large that the lift performance is not expected to be diminished by laminar separation [12]. In the present investigation the combined effect of both aspects of low Reynolds Number and low aspect ratio on T-foil performance for a realistic design is to be confirmed in terms of similar research on two dimensional low Reynolds number foils [13-16] and low aspect ratio lifting wing theory. It was expected from previous investigations that this model scale T-Foil will perform acceptably as a control surface on the bow of a 2.5 m hydro-elastic segmented catamaran model, but the precise detail of the lifting performance needs to be known. Whilst the primary application considered here is to the INCAT Tasmania wave piercing configuration, similar ride control systems can of course be applied also to other types of vessels such as Trimarans and SWATHs. Foil immersion is in general sufficiently deep that Froude number is not significantly relevant to the performance of a submerged T-foil.

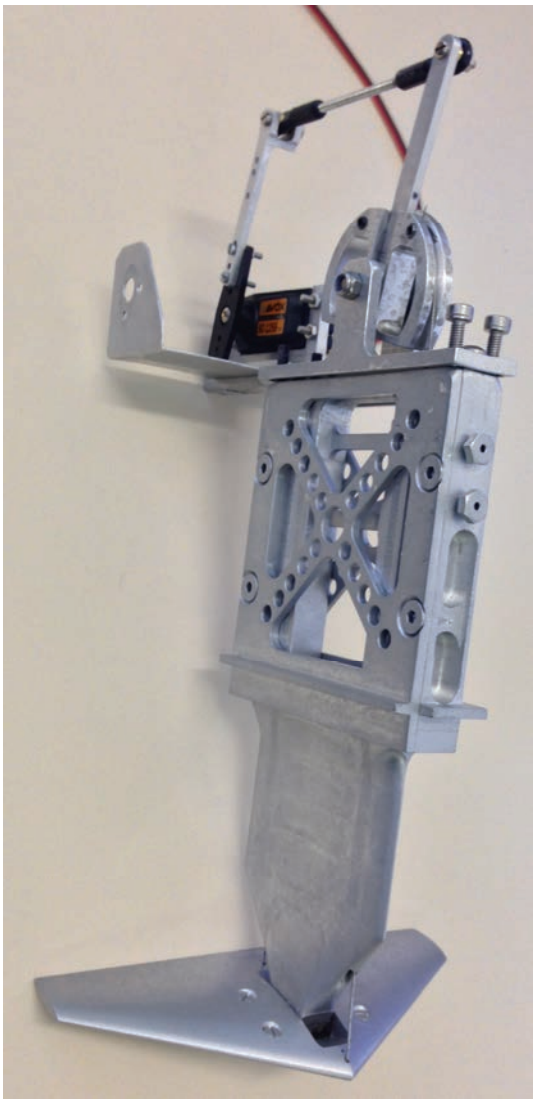

Figure 2: Electrically activated model T-foil.

2. APPARATUS AND INSTRUMENTATION

All the experimental tests were carried out in a closed circuit circulating water tunnel in the University of Tasmania Hydraulics Laboratory (Figure 3). The water

tunnel has a working section with length of 1000 mm, width of 600 mm and a usable depth of 200 mm. The T-Foil model tests needed to be conducted in an open working section so that the free surface was at atmospheric pressure. When operated with an open working section, the water tunnel had not previously achieved velocities above 1.2 m/s with an acceptable flow quality [6]. However, a significant increase of velocity was achieved in the flow by Bell et al [6] using a flow constriction flap (Figure 5). A maximum flow velocity of 2.7 m/s was achieved by changing the angle of the constriction flap as well as water depth.

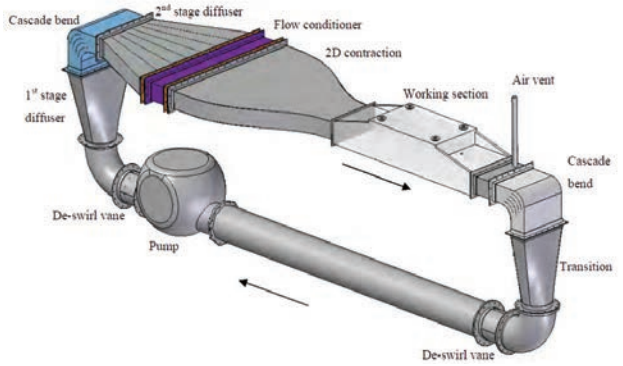

Figure 3: University of Tasmania water tunnel (from Barton [17]).

Figure 4: Load cell set-up on top of the T-Foil vertical strut.

T-foil lift and drag force measurements were carried out using an AMTI 6 Degree of Freedom (DOF) load cell. The load cell was assembled on top of the T-Foil as shown in Figure 4. Figure 5 shows the set-up of the T-Foil and the load cell in the water tunnel. Using a LabVIEW program, the load cell output signals were acquired by a National Instruments (NI) PCI-6221 DAQ card through an AMTI amplifier.

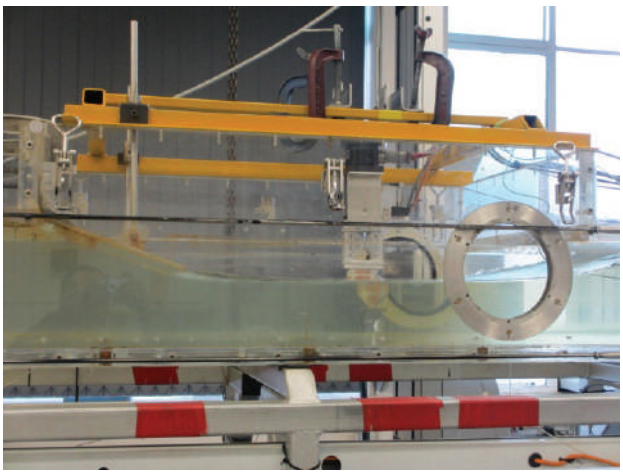

Figure 5: T-Foil and load cell set-up in the circulating water tunnel (flow is left to right).

A stepper-motor was used to activate the T-Foil and a potentiometer was used to measure the angular position of the T-Foil control surface. A National Instruments (NI) 9174-USB compact DAQ (cDAQ) chassis with two NI modules, NI 9263 Analogue Output (AO) and NI 9201 Analogue Input (AI), was used whilst running LabVIEW for both static and dynamic tests. The T-Foil angle of attack was demanded through the NI 9263 AO module and the NI 9201 AI module was used to acquire the potentiometer voltage in order to measure the actual instantaneous T-Foil angle of attack. The channel related to the potentiometer voltage in the NI 9201 AI module was directly connected to an AI channel of the NI PCI-6221 DAQ card in order to measure the true T-Foil angle of attack during force measurements.

3. CALIBRATION

Calibrations of the stepper-motor and the potentiometer were carried out in order to find a relationship between demand voltage for the stepper-motor and T-Foil angle of attack as well as a relationship between output voltage from the potentiometer and T-Foil angle of attack. The T-Foil angle of attack was measured by a digital inclinometer with a resolution of 0.05º. The digital inclinometer was calibrated and oriented relative to the apparatus as the T-Foil chord line was parallel to the water surface at 0º. Figure 6 shows the calibration graphs for potentiometer and stepper-motor. The system has good linearity. Equations 1 and 2 show these relationships respectively:

$$\alpha = (57.46 \times V_{out}) - 156.93 \quad (1)$$

$$\alpha = (80.00 \times V_{in}) - 244.00 \quad (2)$$

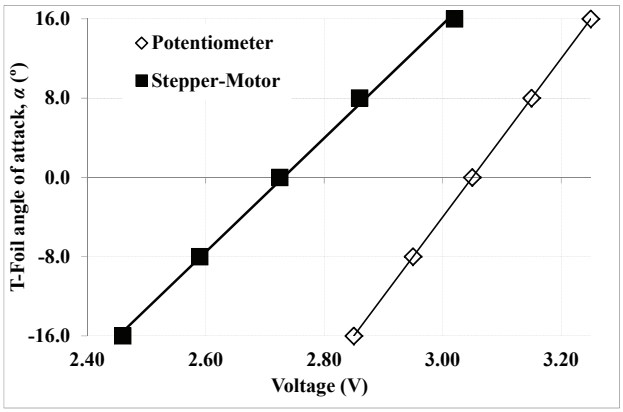

Figure 6: Relationship between T-Foil angle of attack and output voltage from the potentiometer as well as input voltage to the stepper-motor.

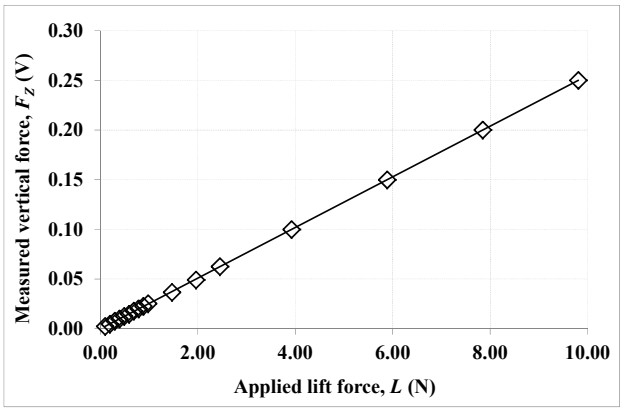

Figure 7: Relationship between lift force and load-cell output voltage measuring force in the vertical z-axis direction, F_z.

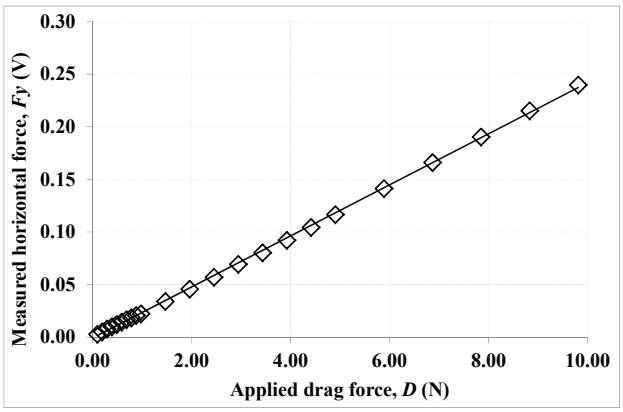

Figure 8: Relationship between drag force and load-cell output voltage measuring force in the horizontal y-axis direction, F_y.

Calibration of the load cell was conducted by applying a static load in the vertical (z-axis) direction of the load cell to find a relationship between lift and output voltage from the channel related to the force in the z-axis direction, F_Z. Similar tests were carried out by applying static loads in the y-axis direction of the load cell to find a relationship between drag and output voltage from the channel related to the force in the horizontal y-axis direction, F_Y.

Figures 7 and 8 show the calibration graphs for lift and drag respectively. These both show good linearity. Equations 3 and 4 show these relationships respectively:

$$F_z = (0.025503 \times L) - 0.000255 \quad (3)$$

$$F_y = (0.024268 \times D) - 0.000871 \quad (4)$$

4. EXPERIMENTAL TESTS AND RESULTS

After installation of the T-Foil and the load cell in the water tunnel, the static tests were carried out at three different water flow velocities consisting of a low speed of 1.82 m/s, a medium speed of 2.30 m/s and a high speed of 2.70 m/s. The flow velocities were selected on the basis of the forward test speeds required for the 2.5 m catamaran model for future testing of motion control response in head-seas. For each water flow velocity, the T-Foil angle of attack was fixed at 10 different angles ranging from -15º to +15º in 3º increments and the magnitude of both lift and drag was measured. The magnitudes of force are shown in Figures 9 and 10 for lift and drag respectively based on a sign convention where the T-Foil angle of attack (α) from port side is positive clockwise with a left to right flow and the generated lift force is positive upwards. These dimensional results can be compared directly with the lift results for stern tabs [6] in assessing the combined performance of a T-foil and stern tabs.

In addition to the static tests, dynamic tests were carried out on the T-Foil. The dynamic tests were carried out in the water tunnel at the three water flow velocities as mentioned above. Three ranges of angle of attack consisting ±5º, ±10º and ±15º were tested for each flow velocity. All these tests were done at 18 different frequencies ranging from 0.5 Hz to 9 Hz in 0.5 Hz increments. The aim of these dynamic tests was to measure the dynamic forces on the T-Foil to compare with static forces as well as to define the T-Foil frequency response. Figure 11 shows a sample of measured dynamic forces at a flow velocity of 1.82 m/s, a frequency of 1.5 Hz and a demand T-Foil incidence (α) range of ±15º.

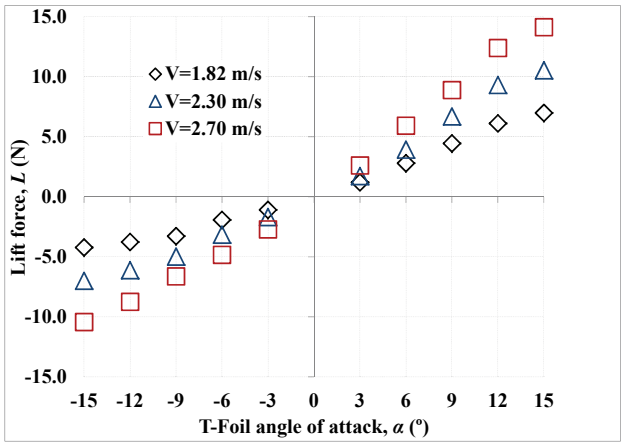

Figure 9: Lift force measured on the T-Foil at fixed angles of attack for static tests undertaken at different water flow velocities.

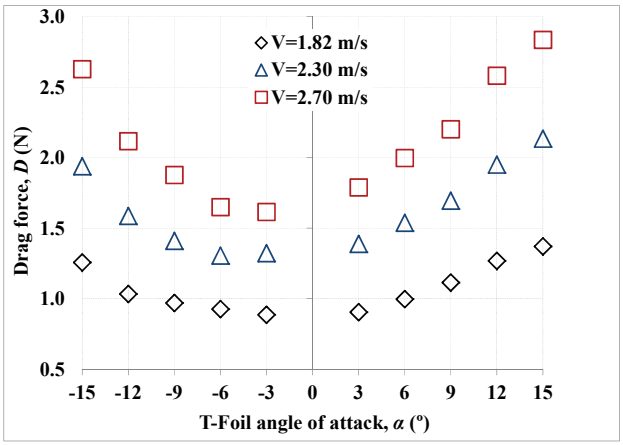

Figure 10: Drag force measured on the T-Foil at fixed angles of attack for static tests undertaken at different water flow velocities.

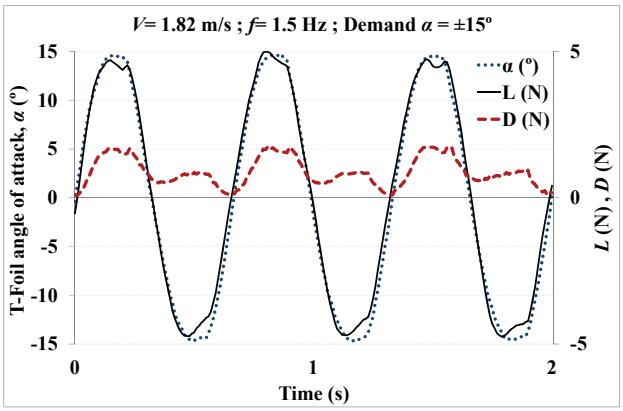

Figure 11: Lift L, and Drag D, forces measured at a flow velocity of 1.82 m/s, frequency of 1.5 Hz and demand T-Foil incidence (α) range of ±15º.

The local form of the peak and trough of the measured lift can be explained on the basis of the mechanical operation of the stepper motor used to drive the T-foil where there is a dead-space in the stepper-motor gearbox as well as slack in the connections between the motor and T-foil.

The results of the frequency response tests included the ratio of the measured angle of attack divided by the demand angle of attack. Also, the phase lag between demand and T-Foil movement was measured. Figures 12 and 13 show these results at the three different flow velocities of 1.82 m/s, 2.30 m/s and 2.70 m/s and also three different demand T-Foil incidence (α) ranges of ±15º, ±10º and ±5º. As can be seen, the ratio of measured angle of attack to the demand angle of attack decreases with increase of frequency in particular above 4 Hz. Also, it can be seen that this ratio is not exactly equal to unity for the low frequencies. However it is close to unity. This phenomenon can be explained in terms of the mechanical operation of the T-Foil linkage set-up. As mentioned before, it was found that there is a dead-space in the stepper-motor gearbox which causes the error. When an angle is demanded for the stepper-motor, its output angle is not exactly equal to the demand angle. This error is relatively more significant for low demand T-Foil incidence (α) range of ±5º as seen in Figure 12. In addition, Figure 13 shows the observed phase lag between measured angle of attack and demand angle of attack. As can be seen the observed phase lag increases with increase of frequency, the linear increase being indicative of a time delay in the control system.

Referring to the previous studies on the INCAT Tasmania hydroelastic segmented model [18], it was found that peak motions and peak loads occurred at the frequencies between 1 Hz and 1.5 Hz. Considering this range of frequencies for a demand T-Foil incidence (α) range of ±10º, which is close to the maximum full-scale range, it can be seen that ratio of measured angle of attack to demand angle of attack is about 0.95 which is acceptable for such a small model test system. Also, the observed phase lag in this range of frequencies is between 10 and 20 degrees which is due to the stepper-motor limitation.

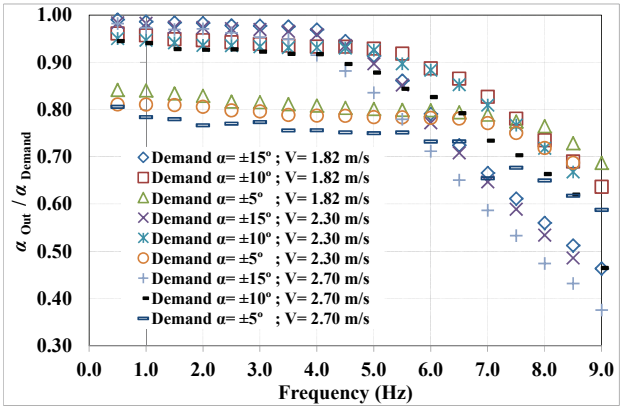

Figure 12: Ratio of measured angle of attack to demand angle of attack at three flow velocities of 1.82 m/s, 2.30 m/s and 2.70 m/s and also three demand T-Foil incidence (α) ranges of ±15º, ±10º and ±5º.

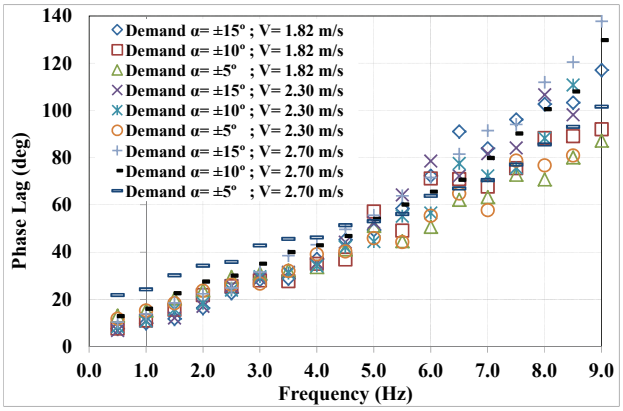

Figure 13: Phase lag at three flow velocities of 1.82 m/s, 2.30 m/s and 2.70 m/s and also three demand T-Foil incidence (α) ranges of ±15º, ±10º and ±5º.

5. COMPARISON OF TEST RESULTS WITH AEROFOIL THEORY AND DATA

5.1. STATIC TESTS

From the measured forces during the T-Foil model tests in the water tunnel, lift coefficients and drag coefficients in the static tests were investigated. Equations 5 and 6 were used to calculate the lift coefficients and drag coefficients respectively:

$$C_L = \frac{L}{\frac{1}{2}\rho V^2 S} \quad (5)$$

$$C_D = \frac{D}{\frac{1}{2}\rho V^2 S} \quad (6)$$

Figures 14 and 15 show the magnitude of lift coefficients and drag coefficients of the T-Foil obtained from the static tests at various water flow velocities. In addition, the lift-to-drag ratio is plotted for different angles of attack in Figure 16.

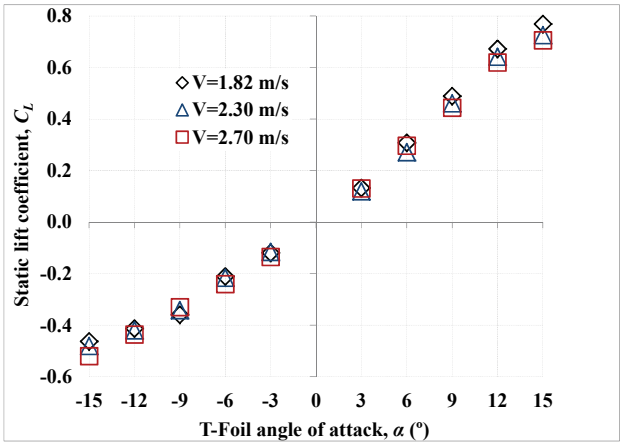

Figure 14: T-Foil static lift coefficient at different angles of attack and various water flow velocities.

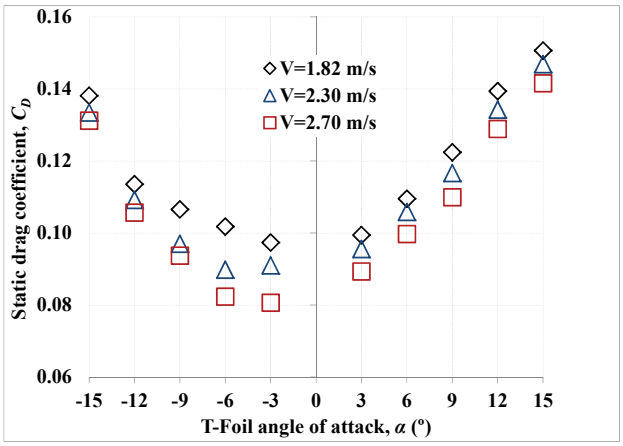

Figure 15: T-Foil static drag coefficient at different angles of attack and various water flow velocities.

As can be seen in Figure 14, the relationship between lift coefficient and angle of attack is not exactly linear. However, the relationship was considered sufficiently close to linear to calculate an average model T-Foil lift-coefficient derivative ($\frac{dC_L}{d\alpha}$) over the incidence range ±15 degrees. This slope was found to be $C_{L\alpha}$ = 2.45 per radian and was considered appropriate to calculate a quasi-static lift coefficient for the dynamic tests as the basis of comparison with measured dynamic lift coefficients.

It is known that the lift curve slope reduces as aspect ratio reduces. This is due to the downwash produced, which reduces the effective angle of attack of the foil. Glauert [19] has investigated the effect of aspect ratio on the slope of the lift curve for both elliptic and rectangular aerofoils. Although the T-Foil used here is not neither elliptic nor rectangular in planform, the foil is approximately intermediate in geometry between elliptic and rectangular planforms. Further, the results obtained using Glauert's equations for aspect ratio of AR = 3.6 varied only slightly, being 3.89 per radian for the rectangular planform and 4.04 per radian for the elliptic planform on the basis of a two dimensional section lift curve slope of 2π per radian. We also note that Ol et al. [14] measured a two dimensional lift curve slope very close to 2π per radian at a Reynolds number of 60,000, significantly less than the Reynolds number of the T-foil tested here which was 105,305 based on the average chord. We therefore can expect that the present T-foil two dimensional section would also have a lift curve slope close to 2π per radian. The possible causes of the rather lower three dimensional $C_{L\alpha}$ = 2.45 per radian measured on the model T-foil are the presence of the T-Foil strut, which obstructs the upper surface, the hinge mount which penetrates the foil to the lower surface and the precise design of the T-foil outboard ends which are approximately rectangular and smoothly contoured. The T-Foil strut in particular may be the cause of asymmetry of the lift curve for positive and negative angles of attack.

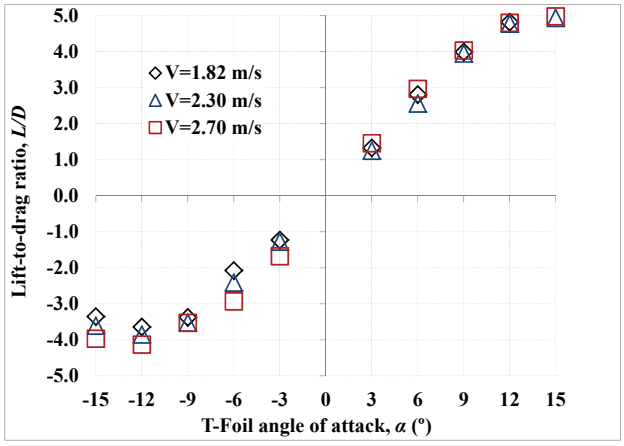

Figure 16: T-Foil lift-to-drag ratio at different angles of attack and various water flow velocities.

5.2. DYNAMIC TESTS

The quasi-static lift coefficient was calculated by multiplying the T-Foil lift-coefficient derivative ($\frac{dC_L}{d\alpha}$) with the measured angles of attack. Figure 17 shows a sample comparison between quasi-static lift coefficient

and dynamic lift coefficient at a water flow velocity of 1.82 m/s, frequency of 1.5 Hz and demand T-Foil incidence (α) range of ±15º. Although this graph shows a good agreement between experimental lift coefficient and quasi-static lift coefficient, there is a deviation at the peaks when the T-Foil reaches the maximum and minimum angle of attack.

As the results presented in Figure 17 were obtained through the experiments, it was decided to compare these results with theoretical calculations. Therefore, Theodorsen's Unsteady Thin Airfoil Theory [20] was applied to conduct the theoretical calculations for dynamic lift effects.

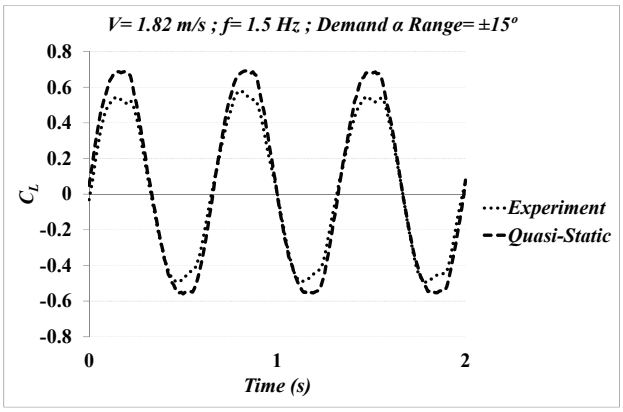

Figure 17: Comparison between experimental lift coefficient and Quasi-static lift coefficient at water flow velocity of 1.82 m/s, frequency of 1.5 Hz and demand T-Foil incidence (α) range of ±15º.

According to the Theodorsen's theory, the lift which contains both circulatory and non-circulatory terms is given by [20] in the form:

$$L = 2\pi\rho VbC(k)\left[\dot{h} + V\alpha + b\left(\frac{1}{2} - a\right)\dot{\alpha}\right] + \pi\rho b^2(\ddot{h} + V\dot{\alpha} - ba\ddot{\alpha}) \quad (7)$$

where the function *C(k)* is a complex-valued function of the reduced frequency *k*, given [20] by

$$C(k) = \frac{H_1^{(2)}(k)}{H_1^{(2)}(k) + iH_0^{(2)}(k)} \quad (8)$$

where $H_n^{(2)}(k)$ are Hankel functions of the second kind, which can be represented in terms of Bessel functions of the first and second kind, given [20] by

$$H_n^{(2)}(k) = J_n(k) - iY_n(k) \quad (9)$$

The function *C(k)* is called Theodorsen's function and is real and equal to unity for the steady case (i.e., for *k*=0) [20].

Three different values for the unsteady lift coefficient are now considered: the Theodorsen prediction based on a steady lift curve slope of 2.45 per radian, direct experimental data from the unsteady water tunnel tests and quasi-static values obtained from the static water tunnel tests. The latter would only be expected to apply at low frequencies. These results are to be compared at two different water flow velocities of 1.82 m/s and 2.70 m/s and three different frequencies of 0.5 Hz, 1.5 Hz and 2.5 Hz. In addition, results are presented for three different demand T-Foil incidence (α) ranges of ±15º, ±10º and ±5º for the flow velocity of 2.7 m/s. Figures 18 to 21 show these results as well as the amplitude response of the foil angle of attack for each case. The left panel of each figure shows the comparison of the demand angle of attack with measured angle of attack. The selected frequencies (0.5, 1.5 and 2.5 Hz) are in the range for which model testing will take place and relatively small magnitude and phase errors are expected between actual movement and demand movement within this as previously discussed.

The results shown for the response amplitude of the angle of attack show a small deviation in the measured range of the angle of attack compared with the demand range of the angle of attack. These results are expected based on the frequency response presented in Figure 12. Figures 18 and 19 show that Theodorsen's theory somewhat under predicts the magnitude of unsteady lift at the highest frequency, but the quasi-static calculation over predicts the magnitude of unsteady lift at all frequencies. These results show that the Theodorsen's theory prediction is relatively close to the experimental magnitude of unsteady lift at a frequency of 1.5 Hz which is the frequency that the INCAT Tasmania model encounters peak motions during tank tests [18]. As can be seen, there is no significant difference in the results between the two different flow velocities (Figures 18 and 19). Thus, it was decided to focus on high water flow velocity of 2.7 m/s as it is close to the design speed of the catamaran model.

Figure 20 shows the results at frequencies of 0.5 Hz, 1.5 Hz and 2.5 Hz, water flow velocity of 2.70 m/s and demand T-Foil incidence (α) range of ±10º. The results shown for the response amplitude of the angle of attack (left panel) show 5% to 10% deviation in the measured range of the angle of attack compared with the demand range of the angle of attack which was expected based on the frequency response presented in Figure 12. The results shown for the unsteady lift coefficient (right panel) show that the Theodorsen theory somewhat over predicts the magnitude of unsteady lift at the lowest frequency, however the quasi-static calculation again over predicts the magnitude of unsteady lift at all frequencies. These results show that the Theodorsen theory prediction is relatively close to the experimental magnitude of unsteady lift at frequency of 1.5 Hz with a discrepancy of 3% at the peak and 11% at the trough.

Figure 21 shows the results at frequencies of 0.5 Hz, 1.5 Hz and 2.5 Hz, water flow velocity of 2.70 m/s and demand T-Foil incidence (α) range of ±5º. The results

shown for the response amplitude of the angle of attack (left panel) show about 20% deviation in the measured range of the angle of attack compared with the demand range of the angle of attack which again was expected based on the frequency response presented in Figure 12. As was explained before, this discrepancy is due to mechanical operation of the T-Foil actuator which introduced a dead-space in the stepper-motor gearbox. This slack causes an error when an angle is demanded for the stepper-motor and its response is not exactly equal to the demand angle. This error is relatively more significant for the low demand T-Foil incidence (α) range of ±5º as the ratio of response deflection to the demand deflection decreases with decreasing range of the demand control angle range. The results shown for the unsteady lift coefficients (right panel) with a ±5º range show that the Theodorsen theory somewhat over predicts the magnitude of unsteady lift at the all frequencies in this case. However the quasi-static calculation is relatively close to the experimental magnitude of unsteady lift at all frequencies. These outcomes are all related to imperfections in the mechanism becoming relatively larger for small movements.

In general, it can be said that there is an acceptable agreement between experimental data and theoretical data. Thus, it is acceptable to use the Theodorsen theory in combination with the quasi-static calculation to predict the dynamic lift coefficients in numerical simulations of motion control systems as the basis for evaluating appropriate control algorithms.

6. CONCLUSIONS

Under steady conditions the effect of low Reynolds number on lift performance is not very significant and the results obtained here show that the model scale T-Foil performs adequately to act as a control surface on the bow of an INCAT Tasmania 2.5m catamaran model. Similar results were found at different water flow velocities and it is evident that the T-Foil performance is not diminished due to the effect of low operating Reynolds Number. The lift curve slope of the T-foil was found to be 2.45 per radian, this being 61% of the value for an ideal foil of the same aspect ratio with elliptic load distribution.

Under unsteady conditions, the magnitude of the measured angle of attack as a ratio to the demand angle of attack decreases as the frequency increases. This ratio is close to unity for the range of frequencies up to 4 Hz for which model testing will be conducted. This outcome can be explained on the basis of the mechanical operation of the stepper motor used to drive the T-foil where there is a dead-space in the stepper-motor gearbox as well as slack in the connections between the motor and T-foil. As a consequence, when an angle is demanded for the stepper-motor, its output angle is not exactly equal to the demand angle. This error is relatively more significant for the lower demand angle range and is due to an absolute error of about ±0.5 degree caused by the mechanical linkage of the model.

The observed phase lag between measured angle of attack and demand angle of attack increases with increasing frequency reaching about 30º at 4 Hz. The phase lag increases approximately in proportion to frequency and thus appears to be caused by time delay and slew rate limitations in the stepper motor actuation system.

It was found that that there is a generally moderately good agreement between the temporal variation of experimentally measured lift coefficients and theoretical lift coefficients derived from a combination of the static lift curve slope and the Theodorsen theory for unsteady lift. This leads to the conclusion that it is acceptable to use the Theodorsen theory for the effect of frequency in combination with quasi-static predictions at low frequency to predict the dynamic lift coefficients during model testing to evaluate control algorithms.

The general conclusion of this investigation is that the unsteady performance of the low Reynolds number model scale T-foil with a relatively low aspect ratio is adequate for application to scale model towing tank tests. It is therefore anticipated that tank testing of a complete 2.5m catamaran model fitted with a model RCS system will lead to the identification of the best motion control algorithms for reducing ship motions and thus contribute significantly to improvement of passenger comfort and reduction of structural loads.

7. ACKNOWLEDGEMENTS

The support of INCAT Tasmania, Revolution Design, the University of Tasmania and the Australian Research Council is gratefully acknowledged.

8. REFERENCES

1. http://www.incat.com.au/#.
2. DAVIS M. R. and HOLLOWAY D. S., "Motion and passenger discomfort on high speed catamarans in oblique seas," *International shipbuilding progress,* vol. 50, pp. 333-370, 2003.
3. HOLLOWAY D. and DAVIS M., "Ship motion computations using a high Froude number time domain strip theory," *Journal of ship research,* vol. 50, pp. 15-30, 2006.
4. JACOBI G., THOMAS G., DAVIS M., HOLLOWAY D., DAVIDSON G. and ROBERTS T., "Full-scale motions of a large high-speed catamaran: The influence of wave environment, speed and ride control system," *International Journal of Maritime Engineering,* vol. 154, pp. A143-A155, 2012.
5. JACOBI G., THOMAS G., DAVIS M. R., and DAVIDSON G., "An insight into the slamming

behaviour of large high-speed catamarans through full-scale measurements," *Journal of Marine Science and Technology,* vol. 19, pp. 15-32, Mar 2014.

6. BELL J., ARNOLD T., LAVROFF J., and DAVIS M., "Measured Loading Response of Model Motion Control Stern Tabs," *Royal Institution of Naval Architects. Transactions. Part A. International Journal of Maritime Engineering,* vol. 155, pp. A1-A7, 2013.
7. DAVIS M., WATSON N., and HOLLOWAY D., "Measurement of response amplitude operators for an 86 m high-speed catamaran," *Journal of ship research,* vol. 49, pp. 121-143, 2005.
8. MATSUBARA S., "Ship motions and wave-induced loads on high speed Catamarans," Doctoral thesis, The University of Tasmania, 2011.
9. SHORE T., "Frequency Response of Motion Controls on INCAT Catamaran Model," Honors Thesis, University of Tasmania, 2011.
10. LAVROFF J., DAVIS M. R., HOLLOWAY D. S., and THOMAS G., "The Vibratory Response of High-Speed Catamarans to Slamming Investigated by Hydroelastic Segmented Model Experiments," *International Journal of Maritime Engineering,* vol. 151, pp. 1-11, Oct-Dec 2009.
11. LAVROFF J., DAVIS M. R., HOLLOWAY D. S., and THOMAS G., "Wave slamming loads on wave-piercer catamarans operating at high-speed determined by hydro-elastic segmented model experiments," *Marine Structures,* vol. 33, pp. 120-142, Oct 2013.
12. EPPLER R., *Airfoil design and data*. Berlin ; New York: Springer-Verlag, 1990.
13. COLMAN J., DI LEO J. M., DELNERO J. S., MARTINEZ M., BOLDES U., and BACCHI F., "Lift and Drag Coefficients Behaviour at Low Reynolds Number in an Airfoil with Gurney Flap Submitted to a Turbulent Flow. Part 1," *Latin American Applied Research,* vol. 38, pp. 195-200, Jul 2008.
14. OL M. V., BERNAL L., KANG C. K., and SHYY W., "Shallow and deep dynamic stall for flapping low Reynolds number airfoils," *Experiments in Fluids,* vol. 46, pp. 883-901, May 2009.
15. PELLETIER A. and MUELLER T. J., "Low Reynolds number aerodynamics of low-aspect-ratio, thin/flat/cambered-plate wings," *Journal of Aircraft,* vol. 37, pp. 825-832, Sep-Oct 2000.
16. TAIRA K. and COLONIUS T., "Three-dimensional flows around low-aspect-ratio flat-plate wings at low Reynolds numbers," *Journal of Fluid Mechanics,* vol. 623, pp. 187-207, Mar 25 2009.
17. BARTON A., "Friction, roughness and boundary layer characteristics of freshwater biofilms in hydraulic conduits," Doctoral thesis, University of Tasmania, 2007.
18. LAVROFF J., DAVIS M. R., HOLLOWAY D. S., and THOMAS G., "Determination of Wave Slamming Loads on High-Speed Catamarans by Hydroelastic Segmented Model Experiments," *International Journal of Maritime Engineering,* vol. 153, pp. A185-A197, Jul-Sep 2011.
19. GLAUERT H., *The elements of aerofoil and airscrew theory*, 2d ed. Cambridge Eng.: University Press, 1947.
20. HODGES D. H. and PIERCE G. A., *Introduction to structural dynamics and aeroelasticity*. Cambridge, England ; New York: Cambridge University Press, 2002.

APPENDICES – Figures: 18-21

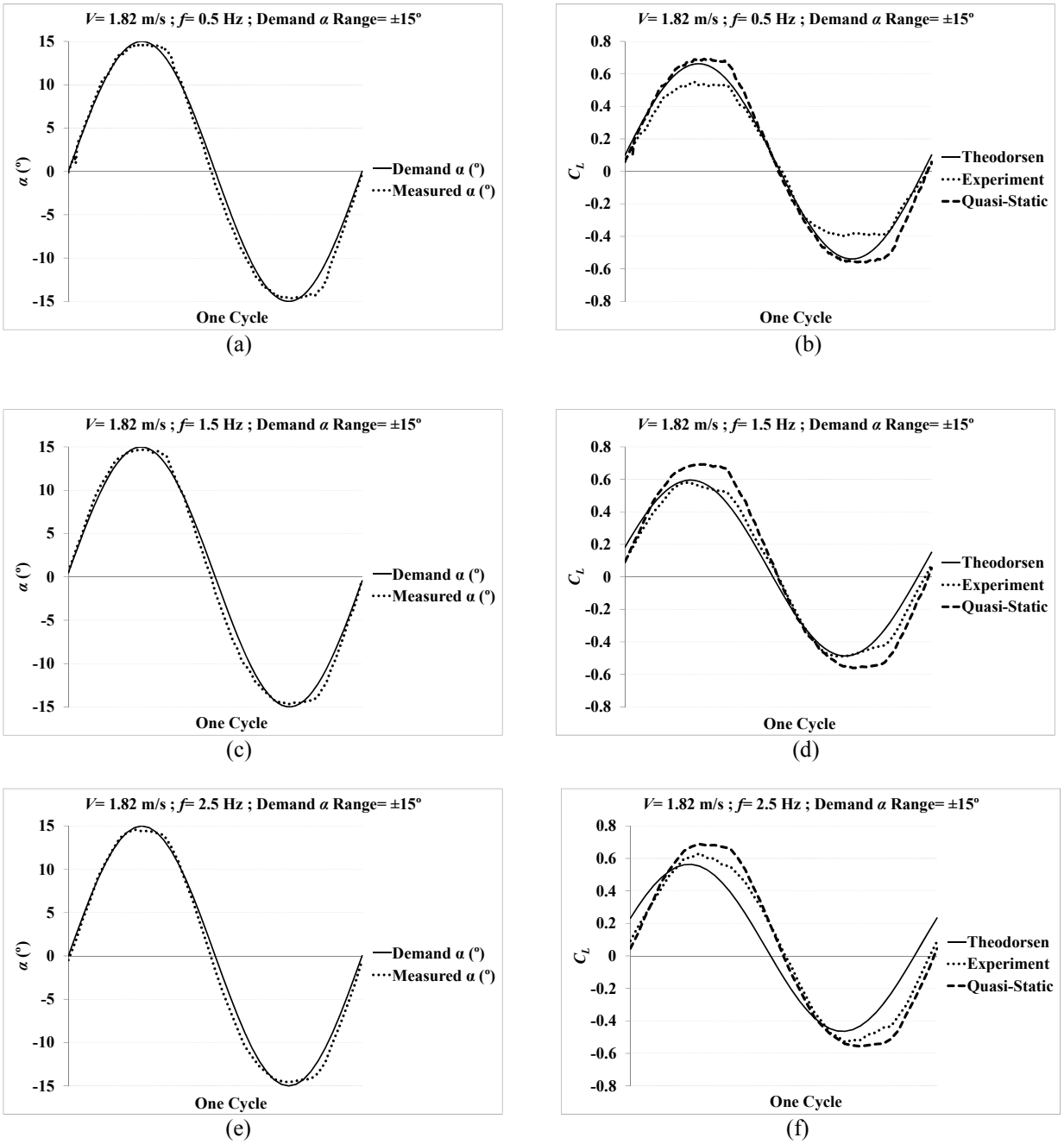

Figure 18: Comparison of T-Foil angle of attack (Left) and lift coefficient (right) at frequencies of 0.5 Hz, 1.5 Hz and 2.5 Hz, water flow velocity of 1.82 m/s with demand T-Foil incidence (α) range of ±15º.

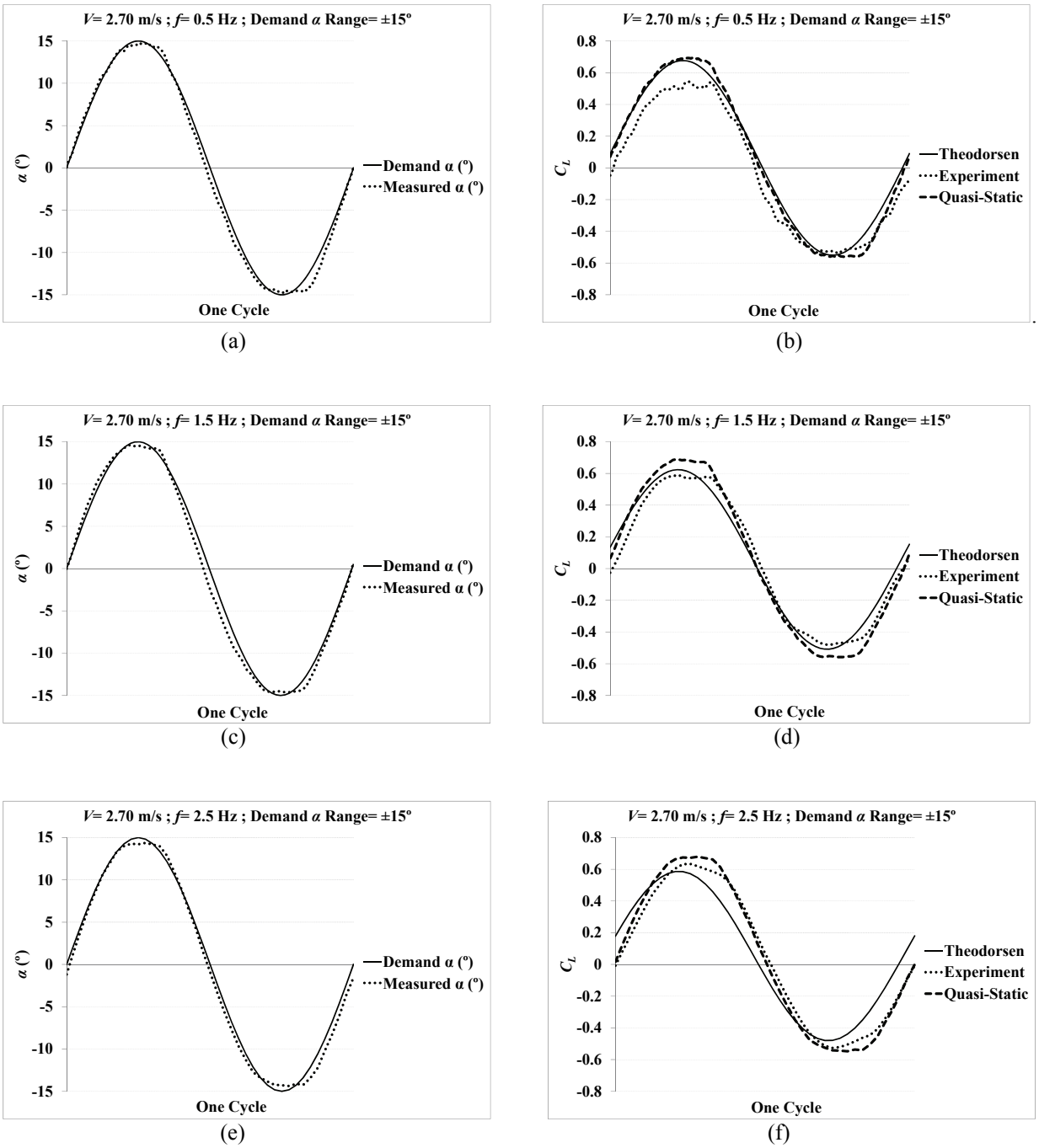

Figure 19: Comparison of T-Foil angle of attack (Left) and lift coefficient (right) at frequencies of 0.5 Hz, 1.5 Hz and 2.5 Hz, water flow velocity of 2.70 m/s with demand T-Foil incidence (α) range of ±15º.

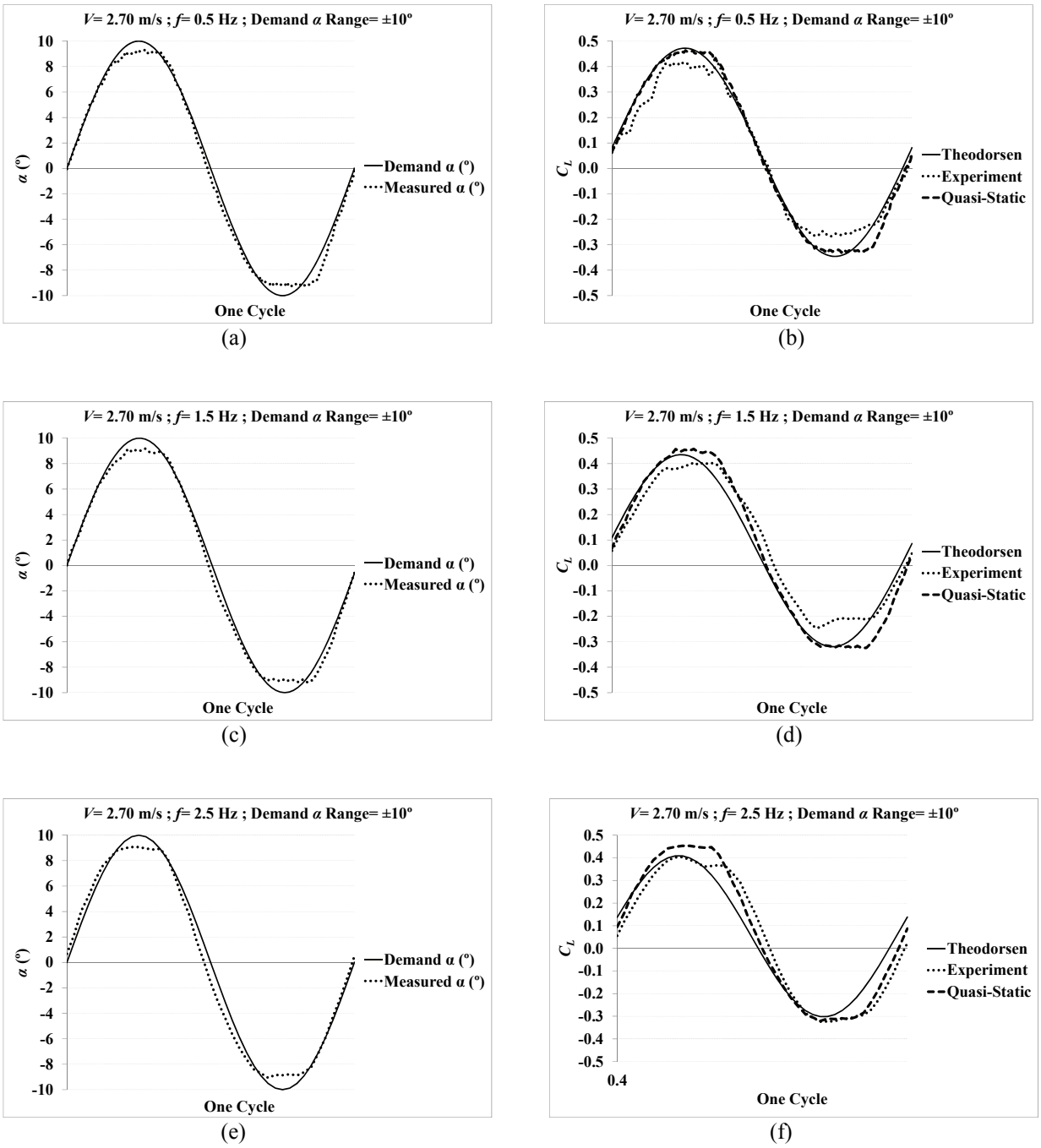

Figure 20: Comparison of T-Foil angle of attack (Left) and lift coefficient (right) at frequencies of 0.5 Hz, 1.5 Hz and 2.5 Hz, water flow velocity of 2.70 m/s with demand T-Foil incidence (α) range of ±10º.

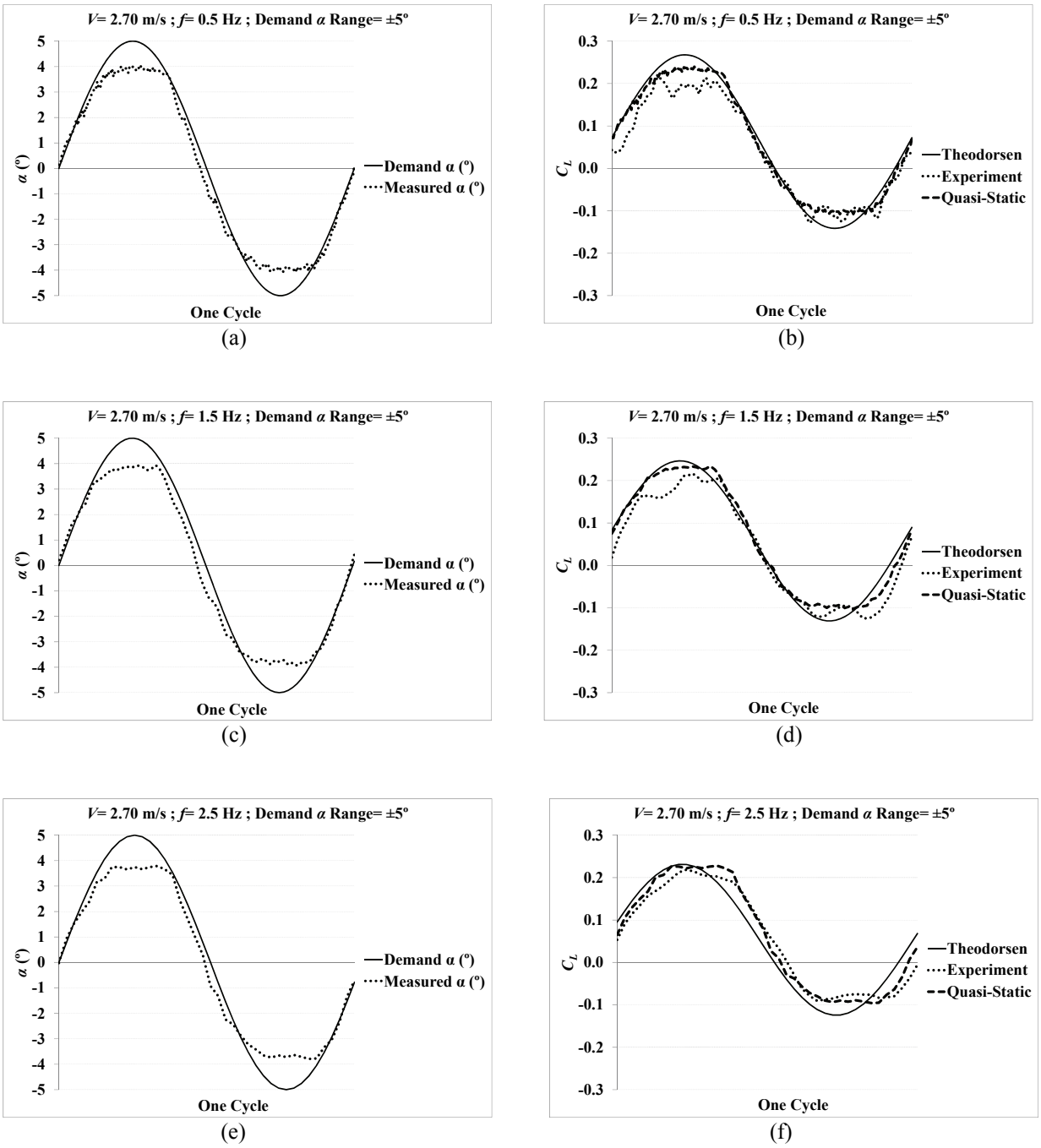

Figure 21: Comparison of T-Foil angle of attack (Left) and lift coefficient (right) at frequencies of 0.5 Hz, 1.5 Hz and 2.5 Hz, water flow velocity of 2.70 m/s with demand T-Foil incidence (α) range of ±5º.